

Removing Temporal Stationary Blur in Route Panoramas

Jiang Yu Zheng and Min Shi
Indiana University Purdue University Indianapolis
jzheng@cs.iupui.edu

Abstract

The Route Panorama is a continuous, compact and complete image representation of scenes along a route. It is generated continuously from reading a preset line in a camera frame that moves along a smooth path. More complicated than the mathematical model of slit scanning, the physical width of a sampling line may yield a temporal blur, named stationary blur, in the route panorama. It is the counterpart of the motion blur and appears at distant scenes. We analyze the sampling of the route panorama, and recover the intrinsic high frequency components from spatio-temporal slit data. The sharpened results enhance the cityscapes archiving and visualization in virtual tour and navigation.

1. Introduction

The route Panorama (RP) is a new type of image media for registering and visualizing cityscapes along streets [1,2]. It samples a properly set pixel line in a camera frame moving along a smooth path [3]. A video camera can be mounted on a moving vehicle to obtain an RP. The plane through the slit and the camera focus, named *plane of scanning* (PoS), is kept vertical in the 3D space (Fig. 1) for scanning streets. Urban scenes are thus projected towards a smooth path so that a long 2D image is formed. The data size of the RP is a small

fraction of the video sequence since it only store a 2D data image slice out of the *spatial-temporal volume*. This is significant for many large-scale applications involving data transmission, rendering, and storage. The key point of the route panorama different from a local panoramic view is to capture image lines at distributed positions along a path. The system has the same principle as a push-broom sensor for terrains [5], but it works on urban scenes with large depth changes from the camera path.

In using a real video camera, the plane of scanning is not absolutely thin. Depending on the resolution, focal length, and the sampling rate of the camera, the route panorama physically employs a series of *Point Spread Functions* (PSF) on the camera path [1,4]. It has the sampling characteristics depending on the scene depth, the vehicle speed, and the path curvature. A phenomenon is the *stationary blur* on distant scenes or scenes on the concave side of the camera path. The degree of the blur increases with the depth as shown in Fig. 1, just as a close scene may yield a motion blur in an image of a translating camera. It is impossible to enhance such a depth variant contrast with a traditional sharpening filter. Most motion deblurring approaches assume that the camera only has a rotation [7,8].

In order to enrich the texture on distant scenes and improve the quality of RP, we propose a method to reduce the stationary blur. By capturing the spatial differentials with the RP in a narrow image stripe



Fig. 1 Sections of route panoramas with scenes at different depths. Stationary blurs are visible.

around the slit, we recover the sharpness that is invariant to the motion blur and stationary blur. The method then sharpens only distant features without affecting close ones, by extracting a depth-dependent high frequency image and adding it to the original RP pixel-wisely. This also preserves the compactness of the RP by avoiding storage of a whole video. On the other hand, our method will not make the contrast of distant scenes sharper than what is possible to obtain in the perspective image.

In the following, we will analyze the sampling process of the RP in Sec. 2. The deblurring algorithm will be given in Sec. 3, followed with results in Sec. 4.

2. Sampling of Route Panorama

2.1. Projection Model of Route Panorama

Conceptually, the video camera constantly takes scenes through a fixed slit l for a route panorama. In the real scanning, pixels on the line are copied from consecutive image frames, and assembled in another image memory $I(t,y)$ to form an RP. Here, t is the frame number and y is the coordinate of l . Ideally, the route panorama employs a parallel-perspective projection, where consecutive PoS are in parallel and perspective projection is employed in each PoS. Among various shape deformations of the projection [1], the parallel PoS keep the width of an object in the RP independent to its depth. Therefore, a distant object is much wider in the RP than in the perspective image.

As the slit sweeps across scenes along a path, the optical flow intersects the slit. Distant features have slow image velocities and close ones have fast image velocities at the slit. The flow direction passing the slit is not guaranteed to be orthogonal. Theoretically, there exists no *Epipolar-plane Image* (EPI) when the camera path is curved [6]. Nevertheless, we can still use a local EPI segment at the slit to explain the behavior of the stationary blur, and use the flow component orthogonal to the slit in our stationary deblurring algorithm.

2.2. When and Where Stationary Blur Appears

In the real scene scanning, the slit has a nonzero physical width and the RP is a connection of narrow perspective projections at discrete positions (Fig 2). The scene depth is classified as the *just-sampling depth*, *under-sampling range* and *overlapped-sampling range*, which have different sampling characteristics. The scenes taken by the PSF at the just-sampling depth (denoted by D_j) can be stitched exactly, just as a normal perspective projection does. For a depth $D < D_j$, consecutive PSFs do not cover the entire space, i.e.,

scenes are *under-sampled*. On the contrary, the space farther than D_j may be covered by multiple PSFs; it is an *overlapped-sampling range*. A point in such a range may contribute to consecutive pixels in the RP, which explains the reason of the *stationary blur*. Because the intensities in a PSF are averaged to yield a pixel value, sampling distant scenes corresponds to filtering the intensity distribution of scenes with a smoothing filter (Gaussian PSF) if $D > D_j$. The resulting horizontal contrasts in the RP are then lower than the original contrasts in the perspective image.

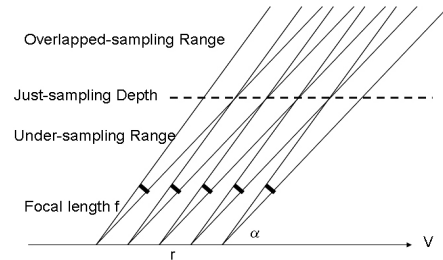


Fig. 2 Real projection of RP using consecutive PSFs.

The sampling of the RP can be characterized by the just-sampling depth, which is related to the PSF, PoS direction α , camera sampling interval r on path and the path curvature κ . The PSF is further determined from the camera resolution (generally fixed) and focal length f . The sampling interval is determined from vehicle speed V and the camera sampling rate m , i.e., $r=V/m$.

A wide-angle lens used for covering larger vertical field of view shortens D_j and increases the stationary blur [9]. Second, the maximum sampling rate of a camera is normally fixed. Slowing down the vehicle to sample details in the close range also reduces D_j and makes distant scenes stationary blurred. Further, setting α to be non-orthogonal to the path for capturing side aspects of buildings increases the stationary blur slightly. It can be proved that the just-sampling depth is

$$D_j(t) = \frac{V(t)}{2m \times \tan \theta + \kappa(t)V(t)} \quad (1)$$

where θ is half of the angle subtended by a PSF, and $\kappa < 0$, $\kappa = 0$ and, $\kappa > 0$ for convex, linear, and concave paths, respectively.

The width of PSF is proportional to the depth. Therefore, a distant edge is filtered by a large smoothing-filter when it is captured by the RP. Its contrast is reduced by a factor, i.e., the depth from the path. If we add a high-frequency component Δ to the RP to enhance the contrast, it should be wide and distinct at distant edges since they are wider in the RP than in the images. Such a component is unable to be extracted from differentiating a severely blurred RP.

3. Removing Stationary Blur in RP

3.1. Image Model of Route Panorama

In analyzing the slit scanning, we focus on a narrow EPI (x - t slice) intersecting the slit at height y (Fig. 3), since it is still possible to process under the hardware restriction. An image and an RP are depicted, and a translating point leaves a non-vertical trace in such an EPI. The image velocity of the point is proportional to the camera moving speed and inversely proportional to the point depth. Denoting the angle between a point trace and the x axis by ϕ , a close point moving fast in the image has a small slope and a distant point has a steep trace. A point at infinity has a vertical trace ($\phi=\pi/2$).

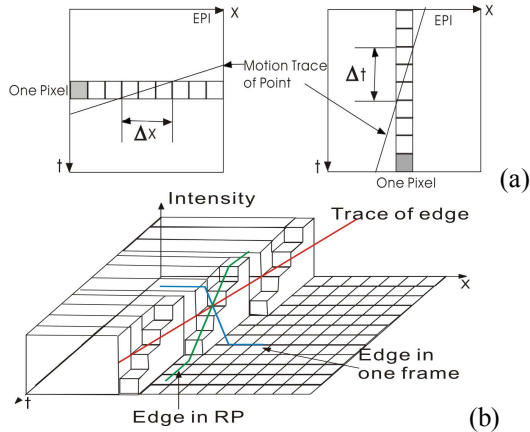


Fig. 3 Motion blur in the image and stationary blur in the RP. (a) Point traces in EPI. Horizontal and vertical pixels indicate the locations of an image and an RP, respectively. (b) Trace of a step edge in EPI shown by its intensity distribution.

The trace of a close edge point may sweep across several (Δx) pixels in the frame during the camera exposed time. The edge intensity thus contributes to multi-pixels in the image, which forms a motion blur [6]. On the contrary, a slow-moving edge retains at the same image position for several sampling instances (Δt). The point is captured repeatedly by the slit. This causes a *stationary blur*, along the t axis in the RP. Distant objects appear to be *stationary-blurred* because of their slow image velocities.

3.2 Deblurring from Spatio-temporal Contrast

If distant scenes are severely blurred in the RP, small details are lost irreversibly. Many sharpening methods in rich literatures only use distinguishable information, by calculating the second derivative of the image and subtracting it from the original image. In the RP, however, features are not equally blurred (but

depending on their depths). We thus compensate the sharpness in the time domain by employing the spatial differential from the original images.

We seek an intrinsic contrast at an edge affected neither by the motion blur nor by stationary blur. As shown in Fig. 4, a step edge of the intensity on a 3D surface is captured in the image as an intensity slope, since it is sampled by PSFs with a physical width. Upon that, a motion blur flats the slope further in the image (slope 2 in Fig. 4a), if the camera shutter is slow. At the same time, stationary blur may happen in the RP (slope 1 in Fig. 4a). Nevertheless, the highest contrast is in the gradient direction of the trace in the EPI, i.e., slope 3 in Fig. 4a. Hence, we refer to the high frequency component orthogonal to the trace direction for RP deblurring.

In the EPI of a particular height, the gradient vector, $G(x, t)$, can be expressed as

$$g(x, t) = \sqrt{\left(\frac{\partial I(x, t)}{\partial x}\right)^2 + \left(\frac{\partial I(x, t)}{\partial t}\right)^2}$$

$$\alpha(x, t) = \tan^{-1}\left(\frac{\partial I(x, t)}{\partial t} / \frac{\partial I(x, t)}{\partial x}\right) \quad (2)$$

where $g(x, t)$ is the magnitude and $\alpha(x, t)$ is the orientation. The magnitude, also the derivative of $I(x, t)$ along direction α ($\alpha=\pi/2+\phi$), is calculated by

$$g(x, t) = I_\alpha(x, t) = \frac{\partial I(x, t)}{\partial x} \cos \alpha + \frac{\partial I(x, t)}{\partial t} \sin \alpha \quad (3)$$

The second derivative of $I(x, t)$ in α direction then is

$$g_\alpha(x, t) = g_x(x, t) \cos \alpha + g_t(x, t) \sin \alpha \quad (4)$$

which is the reliable high frequency component we want to refer to. Accordingly, we have

$$g_x(x, t) = g_\alpha(x, t) \cos \alpha, \quad g_t(x, t) = g_\alpha(x, t) \sin \alpha \quad (5)$$

On the other hand, the projection of the gradient onto the t axis is calculated from Eq. 3 as

$$g_t(x, t) = \frac{\partial g(x, t)}{\partial t} = \frac{\partial^2 I(x, t)}{\partial t \partial x} \cos \alpha + \frac{\partial^2 I(x, t)}{\partial t^2} \sin \alpha \quad (6)$$

Combining Eqs. 5, 6, we obtain

$$g_\alpha(x, t) \sin \alpha = \frac{\partial^2 I(x, t)}{\partial t \partial x} \cos \alpha + \frac{\partial^2 I(x, t)}{\partial t^2} \sin \alpha \quad (7)$$

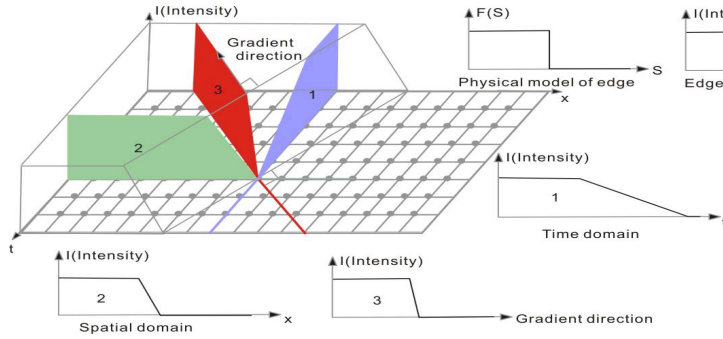
Modifying Eq. 7, we obtain $g_\alpha(x, t)$

$$g_\alpha(x, t) = \frac{\frac{\partial^2 I(x, t)}{\partial t \partial x}}{\tan \alpha} + \frac{\partial^2 I(x, t)}{\partial t^2} = -\frac{\partial^2 I(x, t)}{\partial t \partial x} \tan \phi + \frac{\partial^2 I(x, t)}{\partial t^2} \quad (8)$$

In the same way, we obtain $g_\alpha(x, t)$ from Eq. 3 by taking the second differential along the x axis, which results in

$$g_\alpha(x, t) = \frac{\partial^2 I(x, t)}{\partial x^2} + \frac{\partial^2 I(x, t)}{\partial x \partial t} \tan \alpha = \frac{\partial^2 I(x, t)}{\partial x^2} - \frac{\partial^2 I(x, t)}{\partial t \partial x} \frac{1}{\tan \phi} \quad (9)$$

Now, we can figure out a high frequency component Δ for edge enhancement in the RP. Because the second



Some edges are blurred out at distance end.

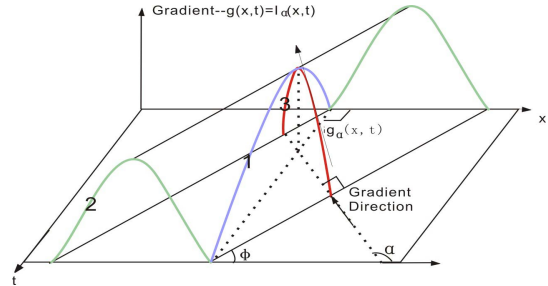


Fig. 4 Behavior of a moving edge in the EPI. (a) Intensity distribution. (b) The first differentials at the edge. Contrasts “1” in the RP, “2” in the image, and “3” along the gradient direction.

derivative $\frac{\partial^2 I(x,t)}{\partial t^2}$ is the high frequency component

already contained in the RP, only

$$\Delta = g_\alpha(x,t) - \frac{\partial^2 I(x,t)}{\partial t^2} \quad (10)$$

is necessary to be added to the RP pixel-wisely to achieve contrast $g_\alpha(x,t)$. Therefore, Δ is calculated in two ways according to Eq. 8, 9, as

$$\Delta_1(x,t) = -\frac{\partial^2 I(x,t)}{\partial t \partial x} \left(\frac{\partial I(x,t)}{\partial x} / \frac{\partial I(x,t)}{\partial t} \right) = -I_{xt} \frac{I_x}{I_t} \quad (11)$$

$$\Delta_2(x,t) = \frac{\partial^2 I(x,t)}{\partial x^2} - \frac{\partial^2 I(x,t)}{\partial t \partial x} \frac{1}{\tan \phi} - \frac{\partial^2 I(x,t)}{\partial t^2} = I_{xx} - I_{tt} - I_{xt} \frac{I_t}{I_x} \quad (12)$$

where $I_{tx} = I_{xt}$. Although Δ_1 and Δ_2 are equal, their values are stable or sensitive in different depths. For a very distant depth ($\phi \gg \pi/4$), I_{xt} is small and we may not obtain sufficient levels for Δ_1 in Eq. 11, even it is scaled by a large I_x/I_t . Within a very close range ($0 < \phi < \pi/4$), Δ_1 has a stable value. On the other hand, three terms in Eq. 12 are hard to balance for a small Δ_2 , if the employed differential operators are not consistent in size and coefficient. At the just-sampling depth ($\phi = \pi/4$), Δ_1 and Δ_2 are equal because $I_{xx} = I_{tt}$ and $I_t = I_x$. This ensures a smooth Δ measure at all depths. In conclusion, we use Δ_2 in the overlapped-sampling range and Δ_1 in the under-sampling range, respectively.

4. Experiments

In order to verify performance of our approach, ideal step edges are synthesized at all depths ($D \in [0 \sim 256m]$ with 1m interval) for exploring the motion and blurring behavior. A five-pixel array samples an edge 15 times, as it moves across the edge. A temporal intensity profile (RP with 15×1 pixels) is obtained. Stacking the temporal profiles with respect to the depth forms a depth-contrast image (15×256 pixels). Fig. 5(a) shows four depth varying intensity images where the just-sampling depths are set at 8m, 16m, 32m, and 64m, respectively. We can notice that the stationary blur spreads out as the depth increases.

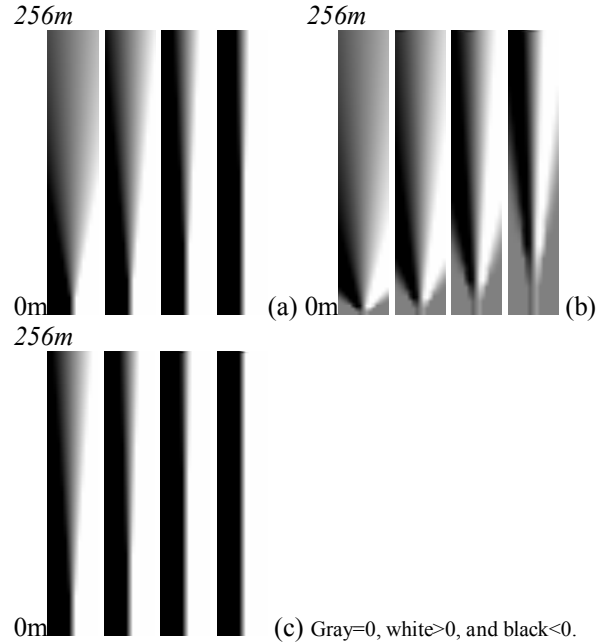


Fig. 5 Removing stationary blur on synthetic edges. (a) Edges at whole depths projected to RPs to form depth-contrast images, examined for four just-sampling depths. (b) Computed high frequency component Δ_s to each in (a). (c) Sharpened edges across the whole ranges by pixel-wise adding of (b) to (a), respectively.

The high-frequency components Δ are computed for all the depths using Eqs. 11, 12. These components (pencil like images in Fig. 5(b)) have less effects at close edges, but change distant contrasts in wide scopes. They are added to the original depth-intensity images in Fig. 5(a) respectively to yield sharpened edge contrasts in Fig. 5(c). It verifies that the proposed approach works for features at different depths under different settings of just-sampling depths.

To obtain differentials $I_x(t,y)$ and $I_t(t,y)$ at the slit, a local operator with size 5×3 is used spatially and temporally to reduce the noise. Second differentials $I_{xx}(t,y)$, $I_{tt}(t,y)$, and $I_{xt}(t,y)$ are also obtained with 5×3 size filters with different coefficients in the *spatio-temporal brick* $I(x,t,y)$ (much narrower than the spatio-temporal volume).

For the real data scanned by a moving camera, five pixel lines centered at the slit are involved in the calculation of the spatial differentials. Only the RP and the spatial differential images are saved to maintain the data compactness of RPs. Figure 6(b) displays Δ image where distant features in Fig. 6(a) have more distinct changes than close ones for the adding operation. Although the enhanced trees after adding Δ is not significantly visible (Fig. 6(c)) because of the texture, the contrasts are consistent to that in the perspective image. Traditional sharpening methods enhance the image without considering the depth. In the second differentials (Fig. 6(d)) computed from Fig. 6(a), close scenes are sharpened while distant scenes are unchanged. Another set of real data is displayed in Fig. 7. By multiply different coefficients to Δ , we obtain different sets of sharpened results; all of them are depth dependent.

5. Conclusion

This work proposed an approach to remove the temporal stationary blur from the route panorama for cityscape visualization. It incorporates the spatial differentials at the sampling slit in the video frames as the route panorama is scanned, and sharpens the scenes automatically according to their depths. The data size is kept small for the route panorama. The algorithm has been examined on synthetic and real data to show its effectiveness.

References

- [1] J. Y. Zheng, Digital Route Panorama, IEEE Multimedia, 10(3), 57-68, 2003.
- [2] J. Y. Zheng, M. Shi Mapping cityscapes into cyberspace for visualization, Journal of Computer Animation and Virtual Worlds, 16(2), 97-107, 2005.
- [3] J. Y. Zheng, S. Tsuji, Panoramic Representation for route recognition by a mobile robot, IJCV, 9, (1), 55-76, 1992.
- [4] M. Shi, J. Y. Zheng, A slit acquiring depth of route panorama based on stationary blur, IEEE CVPR, 1, 1047-1054, 2005.
- [5] R. Gupta, R. Hartley, Linear pushbroom cameras, IEEE PAMI, 19(9), 963-975, 1997.
- [6] P. Rademacher, G. Bishop, Multiple-center-of-projection images, ACM SIGGRAPH 98, 199-206.

- [7] M. Ben-Ezra, S. Nayar, Motion deblurring using hybrid imaging. IEEE CVPR03, 1, pp. 657, 2003.
- [8] M. Potmesil, I. Chakravarty, Modeling motion blur in computer-generated images, SIGGRAPH 83, 389-400.
- [9] J. Y. Zheng, S. Li, Employing a fish-eye camera in scanning scene tunnel, 7th ACCV, 1, 509-518, 2006.
- [10] J. Y. Zheng, Y. Zhou, P. Mili, Scanning scene tunnel for city traversing, IEEE Trans. on Visualization and Computer Graphics, 12(2), 155-167, 2006.

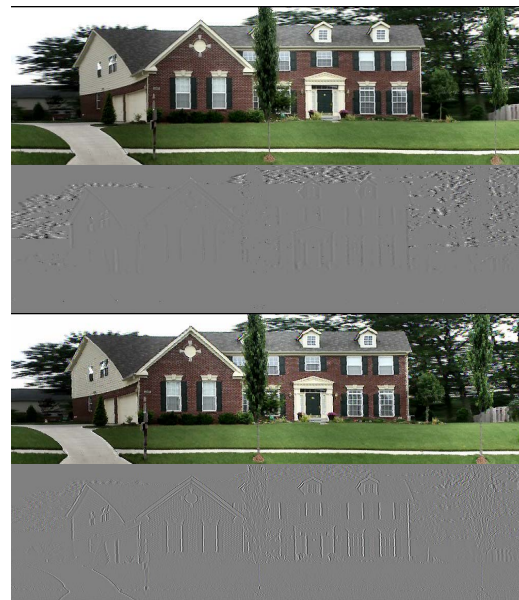


Fig. 6 Recovering sharpness of a section of RP. (a) Original RP. (b) Δ image (gray=0). Distant features behind the house are more enhanced than close features. (c) Recovered RP. (d) For comparison, an enhancement image obtained from the RP with a Laplacian operator is displayed. Only close features are sharpened.

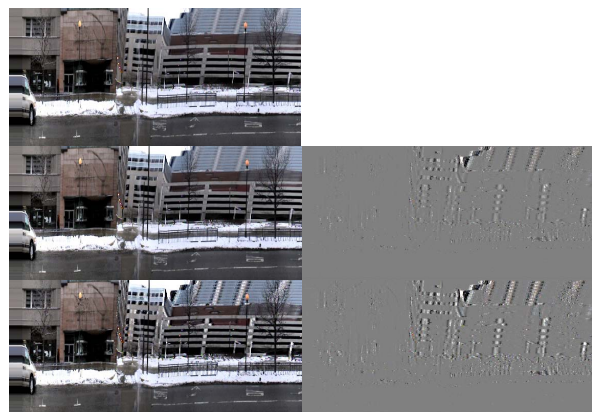


Fig. 7 Enhancing distant features. (a) Original RP with planes at three major depths. (b) Enhanced result by adding Δ image (c) Exaggerated enhancement by adding $2 \times \Delta$ image.